Contents

1 Introduction

2 Methods

VLS, RIE etching FIB, Pt-deposition
  MD BCA, MC Ausgiebige Verwendung von *iradina* [BR11]

3 Sputtering of Nanostructures

When an energetic ion hits a solid target the ensuing collision cascade will displace some of the target atoms from their original positions. The energy lost by the ion in these collisions is called "nuclear" energy loss. A displaced target atom can either become an interstitial, if it stays within the target volume, or be sputtered if it has sufficient energy to leave the solid. The energy required to leave the target is the surface-binding-energy.

4 High Doping Concentrations in Nanostructures

5 Plastic Flow in Nanostructured Silicon

It was mentioned before that within the "wiring quantum dots" project Si nanowires where irradiated with As^+ and In^+ and/or Ga^+ so that in a subsequent annealing step $Si-GaAs$ or $Si-InGaAs$ hetero-structures could be formed. Markus Glaser, the Ph.D. student responsible for this part of the project, had developed a good habit of making SEM images of the same individual wires after each process step. We thus noticed, that the Si nanowires shrank quite dramatically during the irradiation with $\approx 100\,keV$ In^+, Ga^+ and As^+ at room temperature. Two examples of this can be seen in figure $\color{red}Figure$??. A look into literature revealed that this behavior has so far not been reported for irradiation of Si at such low ion energies. A thorough investigation might be worthwhile. Similar Si nanowire arrays as the ones used for the sputtering experiment were thus systematically irradiated with Ar^+, making SEM images after each irradiated fluence to observe and quantify the deformation. Ar was chosen for the irradiation to avoid any chemical effects and because it has a comparable mass to Ga and As.
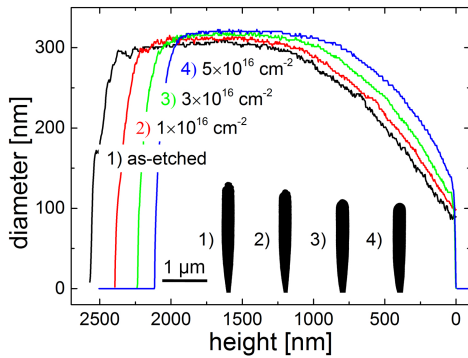

Figure 5.1: Graphs of the diameter over height of a single Si nanowire irradiated with increasing fluences of $100\,keV\,Ar^+$ ions. The black insets show the profiles of the nanowire after the respective fluences extracted from SEM images. In both illustrations the shrinking and widening of the wire is clearly visible.

Using the algorithm described in the sputter yield chapter, the profiles for the irradiated nanowires could be extracted. In figure 5.1 the black, red, green and blue lines indicate the height dependent diameter of a single wire before and after irradiation with $100 \, keV \ Ar^+$ up to fluences of 1, 3 and $5 \times 10^{16} \, cm^{-2}$ respectively. In this graph, as well as in the inset black profiles, the reduction of the height by $\approx 500 \, nm$ and an increase of the diameter, especially at the base, can be clearly seen. The deformation is only seen with irradiation at room-temperature where Si amorphization threshold of $10^{14} \, ions/cm^2$ for $100 \, keV \ Ar^+$ is very low.

The deformation of the nanowires can be roughly quantified by fitting a linear trend to the fluence dependence of the height of the wires. This yields an average of 3% shrinkage per $10^{16} \, ions/cm^2$. Due to outliers with larger deformation the values obtained for the 21 nanowires investigated have a large standard deviation of $\pm 3\%$ shrinking per $10^{16} \, ions/cm^2$. A more thorough investigation of the deformation is possible by also accounting for the height dependence of the diameter seen in figure 5.1. On average a certain number of atoms are displaced by a certain distance along the height z of the nanowire per ion. Considering only the movement along the height z, a mass-transport rate (MTR) can be calculated according to equation 5.1:

$$
\begin{aligned}
MTR_{(1 \to 2)} &= [^1N \cdot {}^1z_c - {}^2z_c \cdot {}^2N - (^1N - {}^2N) \cdot {}^2z_c]/N_{ion} \\
&= {}^1N \cdot (^1z_c - {}^2z_c)/N_{ion}
\end{aligned}
\tag{5.1}
$$

Figure 5.2: Illustration of the mass-transport rate calculation. Displacing ^1N atoms from their average height ^1z_c to the average height ^2z_c requires the same mass-transport, as moving $\hat{N}$ from $\hat{z}_c$ to ^2z_c, taking into account the sputtered atoms $^1N - {}^2N$.
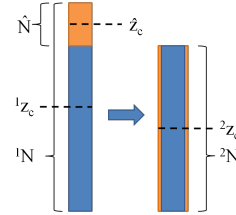
In equation 5.1 and figure 5.2, $^{1/2}z_c$ is the height of the center of mass. The top left index indicates before (^{1}) and after (^{2}) irradiation respectively. The number of atoms at height z_i can be calculated from the local radius r_i. Summing up the height weighted by the number of atoms at that height $z_c \cdot N = \sum_i \pi r_i^2 h \cdot \rho \cdot z_i$ and dividing this by the

total number of atoms $N = \sum_i \pi r_i^2 h \cdot \rho$ in the nanowire gives us z_c. The sums are over all slices i of height $h = 1\,pixel = 2.7\,nm$ (typically) each. The number of ions that hit the nanowire in the irradiation of fluence Φ_{12} between making SEM images 1 and 2 is $N_{ion} = \sum_i \left({}^1r_i + {}^2r_i\right) \cdot sin(45°) \cdot h \cdot \Phi_{12}$. The last term in 5.1 accounts for the influence of sputtered atoms. Just as in the chapter on sputtering, the sputter yield could be calculated by $({}^1N - {}^2N)/N_{ion}$. Figure 5.2 illustrates two interpretations of the MTR calculation. As only the displacement along z is considered, the direct interpretation of equation 5.1 of moving ${}^1N$ atoms from their center of gravity ${}^1z_c$ to a new center of gravity ${}^2z_c$ is equivalent to moving the atoms which are 'missing' at the top of the wire after the irradiation ($\hat{N}$, in orange) from their center of gravity $\hat{z}$ to ${}^2z_c$, and subtracting the sputtered atoms. This evaluation yields an average mass-transport rate of $1.2 \cdot 10^4\,atoms \cdot nm/ion$ with a standard deviation of $7 \cdot 10^3\,atoms \cdot nm/ion$. Again the large standard deviation is due to outliers with larger deformation.

A possible explanation for this behavior can be sought in the linear cascade theory which is applicable for the cascades of $100\,keV\ Ar^+$ in Si. In a collision cascade following an energetic ion impinging a solid, atoms will be preferentially 'knocked-on' along the propagation direction of the impinging ion. This causes an inhomogeneous distribution of interstitials and vacancies and effectively mass is transported 'downstream' along the ion beam. In an amorphous material it is not clear what constitutes an 'interstitial' or a 'vacancy', but a local excess of vacancies can be understood as a locally decreased density, while an interstitial excess corresponds to an increased density. A local density gradient is not stable, since the density of amorphous Si before and after irradiation is not significantly different [PMB04]. Therefore, the density gradient introduces stress in the material which can relax by plastic deformation, possibly enabled by a decreased viscosity due to further ion irradiation $\textcolor{red}{citations}$.

As was shown in the example of sputtering, BCA simulation software can accurately reproduce linear collision cascades. Therefore, comparing the experiments with a simulation with *iradina* can evaluate whether the deformation observed in the experiment can be accounted for by knock-on mass transport. Figure 5.3a shows the simulation volume im-

plemented in *iradina* with $2 \times 2 \times 2\,nm^3$ voxels as a $600\,nm$ long Si cylinder with a diameter of $200\,nm$. The $100\,keV$ Ar^+ ions impinge at an angle of $45°$ to the z-axis. They strike the cylinder distributed uniformly along the y-direction at height $z = 0$. Figure 5.3d shows the resulting distribution of interstitials on the cross-sectional slice through the middle of the nanowire along the xz plane. This can be seen as an approximation for the distribution of the nuclear energy loss and shows the mean extent of the collision cascade. Figure 5.3e shows the same cross-section after subtracting the number of vacancies produced per ion from the number of interstitials interstitials. The excess of vacancies along the impinging plane (blue line in the cross section) enveloped by two red planes of excess interstitials shows that there is a high probability for the ions to hit a target atom with a large impact parameter. This changes the ions path only little and displaces the target atom in an direction perpendicular to the ion beam. Superimposing many collisions along the y direction leads to the formation of one one vacancy rich and two interstitial rich planes. The xy-plane in 5.3b shows the sum over the height z of the difference between interstitials and vacancies plotted to the same color scale. The illustration is dominated by vacancies at the surface of the cylinder which are left behind by sputtered atoms.

The height distribution (summing over the radial xy plane) of the interstitials, vacancies and leaving atoms is shown in 5.3c. As expected, the majority of sputtered atoms originate near the impact height. The lines showing the interstitials and vacancies overlap in this illustration. The vacancies subtracted from the sum of interstitials and leaving atoms is plotted along the height in 5.3f. As a displaced atom, leaving behind a vacancy, is either sputtered or becomes an interstitial, the sum over all heights of of this graph is zero. The strong oscillation around $z = 0$ in 5.3f is caused by the previously discussed displacement of target atoms at an angle almost perpendicular to the ion beam for large impact parameters. This oscillation is very sensitive to the voxel-size as interstitial and vacancy rich regions are superimposed for larger voxels. In effect the voxel size defines a recombination length. On the other hand, the excess of vacancies near the impact point ($\leq 70\,nm$) and of interstitials further down along the ion's path ($\approx 100\,nm$) is not sensitive to the voxel size. It can be used to quantify the knock-on mass transport by multiplying the plotted values by their height and integrating over all heights. The

influence of the short range oscillation immediately around the impact point disappears as here $z \approx 0$ is small. The value obtained from this calculation is $78 \pm 1\, atoms \cdot nm/ion$. Clearly this value is to low to account for the large deformation observed in the experiment where a mass-transport rate of $\geq 1 \times 10^4\, atoms \cdot nm/ion$ was assessed.

As a little excursion, it has to be noted that BCA software typically checks at each collision whether the target atom acquires more energy than the "displacement energy" which is a material specific parameter. If an atom has less than the displacement energy after a collision, it is assumed to remain bound in its place and the energy is converted into lattice vibrations (= heat). The displacement energy is experimentally accessible for crystalline materials by electron irradiation experiments in which the irradiating electron energy is in the order of MeV. From the electrons' impulse and mass the maximum transferred energy can be calculated. The defects produced as a function of electron energy can thus be used to determine a threshold energy for point defects. This value is defined as the displacement energy. For all simulations a reasonable value for crystalline Si, $15\,eV$ was used. As point defects are not well defined in an amorphous medium it is questionable what this value is supposed to mean for them. Therefore, simulations where repeated with the displacement energy set to $0\,eV$. As expected, the number of 'vacancies' and 'interstitials' now produced by the simulation increased dramatically. However, the long range difference between 'vacancies' and 'interstitials' is unchanged. This is an indication that the knock-on mass transport is dominated by the rare events where target atoms are hit directly by the impinging ions. In these cases, a large amount of energy is transferred to the displaced atom leading to a long trajectory within the material. The atoms displaced with lower energies are much more numerous, but travel much shorter distances and in a randomly orientated direction. This is because most of the low energy displaced atoms are generated at the end of a branch of the collision cascade, the orientation of the branch having previously been randomized by higher energy collisions. And/or they originate from collisions with a high impact factor, which lead to a large angle between the incoming particle's and the displaced particle's momentum (as seen in figure 5.3e).

If knock-on mass-transport is not the main contribution to the deformation, the question arises whether the direction of the deformation is related to the ion beam. The question is, whether an irradiation from 'below the substrate' towards an unconstrained end of the nanowire would also shrink the wire, or stretch it out. Nanowires attached to a substrate are obviously not suited to testing this, so a method to irradiate nanowires while rotating them at angles greater than 90° to the
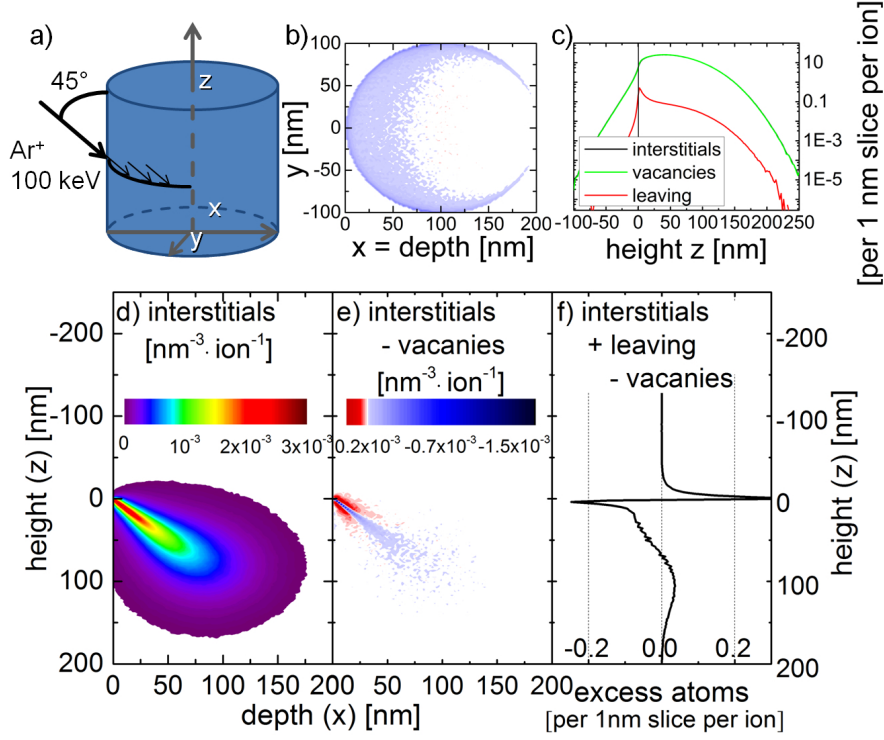
Figure 5.3: a) Illustration of the simulated irradiation geometry. All Ar^+ ions of $100\,keV$ energy hit the nanowire volume at the same height and at an angle of $45°$ with respect to the wire axis z. The created interstitials in the radial cross-section through the middle of the simulated nanowire is shown in d). This distribution is effectively an illustration of the nuclear energy loss. In e) the vacancies are subtracted from the interstitials for the same cross-section. Summing this difference over all heights gives the radial distribution shown in b). The clear dominance of vacancies near the surface is caused by sputtering. The axial profile of the interstitials, vacancies and leaving (sputtered) atoms plotted in c) over the height relative to the impact plane shows, that most atoms are sputtered at the impact height. Note that the plots of vacancies and interstitials overlap. The vacancies subtracted from the sum of interstitials and sputtered atoms plotted over the height in f) shows mass transport along the ions path. Apart from the strong oscillation at the impact height, there is a deficiency of atoms close to the impact height ($\leq 70\,nm$) and an excess centered around $100\,nm$ down from the impact height.

11

ion beam was devised. It is shown in figure 5.4. Using the *Pt*-deposition available in the FIB, a *Si* nanowire grown epitaxially on an *Si* wafer is glued to the micro-manipulator in the FIB. The nanowire is cut from the substrate with the *Ga*-FIB. Using the *Pt*-deposition and *Ga*-FIB, the nanowire is subsequently attached to the tip of a sharpened *Au*-microwire which was previously glued to a wafer for handling and also placed in the FIB chamber. VLS-grown nanowires were used for this experiment as they were readily available in longer lengths ($> 10\mu m$) than the etched nanowires.
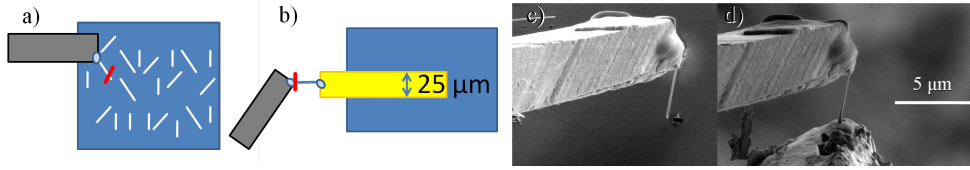

Figure 5.4: Illustration of the nanowire-on-microwire fabrication in a FIB system. The schematic a) and SEM image c) show the wire first glued to the micro-manipulator in the FIB by *Pt*-deposition (light blue ellipse), then cut from the substrate with the *Ga*-FIB (red line). Images b) and d) Illustrate the subsequent gluing to an *Au* microwire with *Pt*-deposition and the final cut with the *Ga*-FIB to release the nanowire from the micro-manipulator.

The nanowire-on-microwire samples consisted of typically $3-5$ nanowires, each attached to an *Au*-microwire and arranged in the irradiation chamber on a rotatable stage at an angle of $135°$ to the ion beam, as shown in figure 5.5a. The alignment of the nanowires to their microwire support was found to be crucial, as any shadowing of a nanowire from the ion beam an one side would lead to extreme bending of the wire. Therefore also only a single wire was found straight enough to evaluate quantitatively for more than on irradiation step. The SEM images of this wire are shown in figure 5.5b-f view from a perspective perpendicular to the axis of rotation and rotated by the indicated angle around this axis. The left SEM images show the uniradiated nanowire, while the center and right images were made after the irradiation of $1 \times 10^{16} \, cm^{-2}$ and $3 \times 10^{16} \, cm^{-2} \, 100 \, keV \, Ar^+$, respectively. The uniradiated wire is straight and $3.9 \, \mu m$ long. The irradiated wire shows some bending, so the length had to be determined from a perspective were the curvature of the wire

is in plane with the image. A fifth order polynomial was fitted to the bent shape and the length of the wire was thus determined to be $3.5\,\mu m$ after $1 \times 10^{16}\,cm^{-2}$ (5.5b) and $3.2\,\mu m$ after $3 \times 10^{16}\,cm^{-2}$ (5.5f). The nanowire thus shrank even though the irradiation was directed towards its free end.
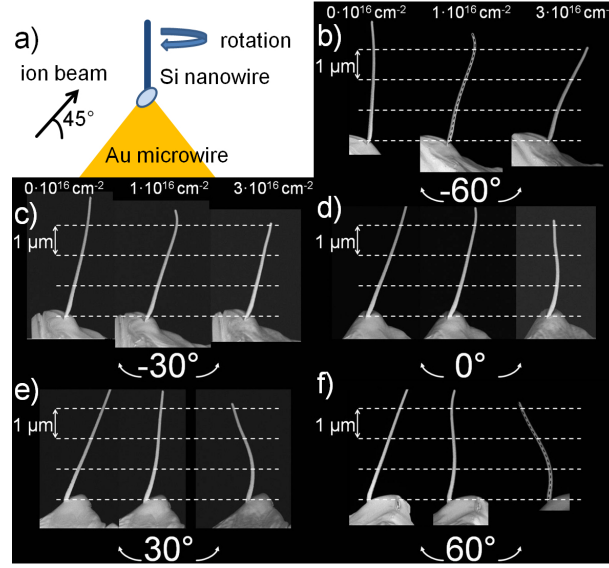

Figure 5.5: a) Illustration of the nanowire-on-microwire irradiation setup. b) - f) SEM images of the same nanowire as-mounted (left SEM images), after irradiation with $1 \times 10^{16}\,cm^{-2}$ (center images), and $3 \times 10^{16}\,cm^{-2}$ (right images) $100\,keV\,Ar^+$ ions. The SEM images where taken with the nanowire rotated by the indicated angle from an angle perpendicular to the angle of rotation. The length of the nanowire after irradiation is determined in b) and f) along the dashed lines.

This experiment shows with certainty that the knock-on mass-transport is not the main contributor to the observed deformation, as it would have to be directed along the ion beam. The discussion of a possible model for the deformation will be easier by addressing similar effects and the way that simulation tools were used to understand them. The BCA MC simulation tools available inherently neglect all collective movement of atoms within the target. As has been shown in the previous two chapters, this may be sufficient for the prediction of sputtering and the ion distribution

in nanostructures. A field of study which has already faced the limitation of neglecting the local temperature in ion irradiation is the irradiation with swift, heavy ions. At energies well beyond MeV the assumption that the dominating effects will be described by binary collisions between the ion and target atoms is false. At these high energies and ion masses a significant amount of energy will be transferred form the ion to the electronic system of the target. Through the relaxation mechanisms of the electronic system a part of this energy will be converted to heat in the lattice. Under certain conditions this will form "ion-tracks" in the target. One approach to understanding the formation and behavior of ion-tracks is to simulate the longitudinal distribution of the deposited ion energy in the target with BCA tools (typically SRIM) and to evaluate the local temperature in a second step by following the deposited energy according to thermodynamic considerations. A good review of such "thermal spikes" can be found in [WKW04]. Such a thermal spike approach was successful at understanding the plastic deformation by swift heavy ion irradiation according to Trinkaus and Ryazanov [TR95] and in the understanding of material properties governing the direction of the deformation [HKW04, HKW05]. When nanoparticles are deformed [SvBvD$^+$00, SvBvD$^+$01, vDSF$^+$01, DPFB01, DPKB03, DDP$^+$04] an adapted version of the model by Trinkaus can be applied and the effect dubbed "ion hammering" [Kla04]. In short, according to this model the local temperature leads to a transient 'liquid' phase in the cylindrical volume of material around the ion's path. Within the cylindrical geometry, the deformation by thermal expansion is anisotropic and because stresses can relax in the low viscosity volume this is a plastic deformation. This is not observed in materials which remain crystalline during the irradiation, as the long range order of the crystal lattice is reinforced upon the recrystallization during cooling. The problem with directly applying this model to the situation at hand is that the total energy density in the collision cascade of $100\,keV\,Ar^+$ in Si is a low $\frac{dE}{dx} = 36\,\frac{eV}{nm}$, of which the electronic energy loss is roughly half. Also for the lowest energy report of plastic deformation of silica nanoparticles by $300\,keV\,Xe^+$ [DPKB03] the energy loss is merely $\frac{dE}{dx} = 120\,\frac{eV}{nm}$ with $20\,\%$ lost to the electronic system. The threshold for ion tracks, however, is set at $\frac{dE}{dx} \geq 1\,\frac{keV}{nm}$ [TR95]!

The alternative to thermodynamic considerations are direct MD simulations, where the trajectory and interaction of every atom or ion in

the simulation volume is followed. This naturally includes all thermal effects, but is obviously limited to a low number of atoms and thus a severely limited volume of material. Additionally also here the accuracy of results depends greatly on finding the interaction potential for all combinations of ions and atoms involved, again especially for low energy interactions, where these potentials are not available, but a topic of research in themselves $CITE$. The investigation of thermal sputtering by MD was already mentioned. Investigations of the self-irradiation of $10\,keV\,Si$ and various metals [?] revealed the formation of nanoscale 'liquid' pockets. The term "liquid" must be used with care as it refers to a thermodynamical state of matter while the simulation timescale does not allow the assumption of thermodynamic equilibrium. Nevertheless, a sufficiently large number of atoms gain much kinetic energy (say 'are hot') to make the assumption of reduced viscosity and other effects safe. The interesting point of this example is, that the energy in the collision cascade was quite low, so that the trajectory of the initiating particle could be accurately simulated according to the BCA. A more recent MD by Baumer et al. takes us a step further in that it predicts plastic deformation in metallic glasses irradiated with high energy neutrons [?]. The collision cascades are initiated in $a\text{-}Cu_{50}Nb_{50}$ by assuming primary knock-on atoms of $475\,keV\,Nb$. This atomistic study explicitly shows that plastic deformation due to thermal expansion and stress relaxation can be anisotropic also in collision cascades which do not have the high energy density and symmetry required by the Trinkaus model [TR95]. Contrary results were obtained by Mayr et al. [MAAA03] where $10\,eV$ to $100\,keV$ recoils of Cu and Ti in $a\text{-}CuTi$ were simulated. That study comes to the conclusion that the viscous flow is dominated by ion induced point defects. It does not propose that knock-on atoms are initiate the deformation, but rather, that thermal effects do not provide the main contribution to the reduced viscosity observed during ion irradiation.

The effect of anisotropic deformation within the collision cascade induced by the irradiation of nanowires is shown in figure 5.6a - c. An approximately ellipsoidal volume of the target material is heated by the collision cascade. It expands, becoming more spherical and the anisotropic deformation is retained after cooling. The superimposition of many collision cascades with a similar effect leads to a net contraction along the
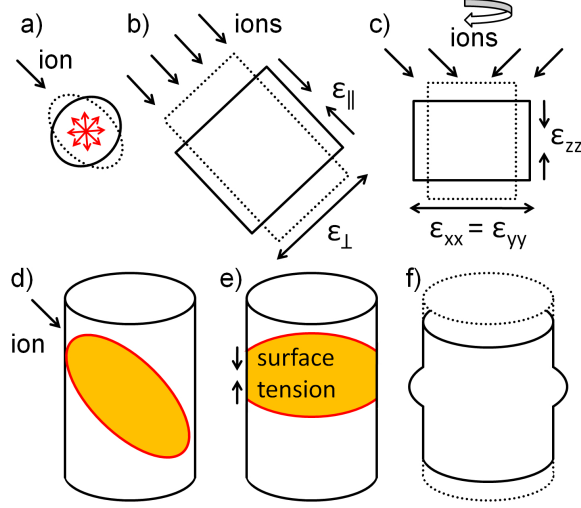
Figure 5.6: a) - c) Illustration of an deformation model analogous to ion hammering. a) The collision cascade from a single impinging ion heats an approximately ellipsoidal volume of the target material. The internal pressure will lead to an expansion towards a more spherical shape, which is retained upon cooling. b) The net effect of many ions is thus a contraction parallel to and an expansion perpendicular to the ion beam. For no change in density $\epsilon_{\parallel} = -2\epsilon_{\perp}$ has to hold. c) Under rotational symmetry this deformation translates to a contraction in the rotational axis z and an expansion in the perpendicular $x-y$ plane with $\epsilon_{zz} = -2\epsilon_{xx} = -\epsilon_{\perp}$. In d) - f) the alternative, surface tension driven deformation is illustrated. The collision-heated volume of target material shown in d). A significant slice of the wire shown in e) thus has a reduced viscosity. The surface energy is reduced by an increase in the local diameter of the wire, leading to a shortened and thickened wire segment shown in f).

ion beam $\epsilon_\parallel < 0$ and an expansion perpendicular to it $\epsilon_\perp > 0$ as shown in 5.6b. To maintain constant density $\epsilon_\perp = -2 \cdot \epsilon_\parallel$. The rotational average of this deformation around the z-axis, as illustrated in 5.6c, works out to be a contraction along the z-axis $\epsilon_{zz} = \frac{1}{2}\epsilon_\parallel$ and a corresponding expansion in the xy-plane for an angle of $\pm 45°$ between the ion beam and the z-axis. The z-axis of course represents the nanowire axis, while the xy-plane is parallel to the nanowire diameter. Thus the deformation rate of $\dot{\epsilon}_{zz} = 3\%$ strain per $10^{16}\,ions/cm^2$ extracted from a linear fit to the reduction of the nanowire height can be transformed into a strain rate parallel to the ion beam of $\dot{\epsilon}_\perp = 6\%$ strain per $10^{16}\,ions/cm^2$. This is much less than the values reported for the studies at higher energies reported in literature. In ref. [DPKB03] $10^{-16}cm^2/ion$ were reported for $300\,keV\,Xe$ in silica nanoparticles and ref. [**?**] even arrives at $10^{-15}cm^2/ion$ with MD calculations in bulk. There are unfortunately no studies published on straining bulk silicon at these low ion energies. The bending of thinned Si-wafers similar to [**?**, **?**] would be measurable with the a straining rate of 6% strain per $10^{16}\,ions/cm^2$ in a layer of $\approx 300\,nm$.

The quantitative discrepancy between the deformation observed in the experiments presented here and published studies may be attributed to the lower ion energy and one may gain confidence in this model due to the qualitative similarity to the MD simulations by Baumer et al. [**?**] also showing deformation anisotropy at low cascade symmetry. However, a further, major concern is the fact that in the presented experiments, the collision cascade is not in bulk, but in a nanostructure were there is not a lot of material around and it is not distributed around the cascade isotropically. An alternative model illustrates that the strong influence of the surface expected in nanowires can also lead to the observed plastic deformation. In figure 5.6d the relation between the nanowire and collision cascade is shown. As there is not much material around, the temperature in a sizable slice of the nanowire will remain elevated for some time [**?**, **?**, **?**, **?**]. In addition the ion irradiation will further reduce the viscosity [**?**, **?**, MAAA03], allowing the surface tension to deform the nanowire by increasing the radius locally. The local increase in diameter reduces the total surface area and thus the surface energy. The wire subsequently becomes shorter and wider as shown in figure 5.6f.

bending citation [BSL$^+$11, BMB$^+$11]

6 Summary and Outlook

test

Bibliography

[BMB+11] Christian Borschel, Maria E. Messing, Magnus T. Borgstrom, Waldomiro Paschoal, Jesper Wallentin, Sandeep Kumar, Kilian Mergenthaler, Knut Deppert, Carlo M. Canali, Hakan Pettersson, Lars Samuelson, and Carsten Ronning. A New Route toward Semiconductor Nanospintronics: Highly Mn-Doped GaAs Nanowires Realized by Ion-Implantation under Dynamic Annealing Conditions. *Nano Letters*, 11(9):3935–3940, September 2011. WOS:000294790200073.

[BR11] C. Borschel and C. Ronning. Ion beam irradiation of nanostructures – A 3d Monte Carlo simulation code. *Nuclear Instruments and Methods in Physics Research Section B: Beam Interactions with Materials and Atoms*, 269(19):2133–2138, October 2011.

[BSL+11] Christian Borschel, Susann Spindler, Damiana Lerose, Arne Bochmann, Silke H. Christiansen, Sandor Nietzsche, Michael Oertel, and Carsten Ronning. Permanent bending and alignment of ZnO nanowires. *Nanotechnology*, 22(18):185307, May 2011. WOS:000288653300010.

[DDP+04] T. van Dillen, M. J. A. de Dood, J. J. Penninkhof, A. Polman, S. Roorda, and A. M. Vredenberg. Ion beam-induced anisotropic plastic deformation of silicon microstructures. *Applied Physics Letters*, 84(18):3591–3593, May 2004.

[DPFB01] T. van Dillen, A. Polman, W. Fukarek, and A. van Blaaderen. Energy-dependent anisotropic deformation of colloidal silica particles under MeV Au irradiation. *Applied Physics Letters*, 78(7):910–912, February 2001.

Bibliography

[DPKB03]   T. van Dillen, A. Polman, C. M. van Kats, and A. van Blaaderen. Ion beam-induced anisotropic plastic deformation at 300 keV. *Applied Physics Letters*, 83(21):4315–4317, November 2003.

[HKW04]   André Hedler, Siegfried Ludwig Klaumünzer, and Werner Wesch. Amorphous silicon exhibits a glass transition. *Nature Materials*, 3(11):804–809, November 2004.

[HKW05]   A. Hedler, S. Klaumünzer, and W. Wesch. Boundary effects on the plastic flow of amorphous layers during high-energy heavy-ion irradiation. *Physical Review B*, 72(5):054108, August 2005.

[Kla04]   S. Klaumünzer. Ion hammering of silica colloids. *Nuclear Instruments and Methods in Physics Research Section B: Beam Interactions with Materials and Atoms*, 215(3–4):345–352, February 2004.

[MAAA03]   S. G. Mayr, Y. Ashkenazy, K. Albe, and R. S. Averback. Mechanisms of Radiation-Induced Viscous Flow: Role of Point Defects. *Physical Review Letters*, 90(5):055505, February 2003.

[PMB04]   Lourdes Pelaz, Luis A. Marqués, and Juan Barbolla. Ion-beam-induced amorphization and recrystallization in silicon. *Journal of Applied Physics*, 96(11):5947–5976, December 2004.

[SvBvD$^+$00]   E. Snoeks, A. van Blaaderen, T. van Dillen, C. M. van Kats, M. L. Brongersma, and A. Polman. Colloidal Ellipsoids with Continuously Variable Shape. *Advanced Materials*, 12(20):1511–1514, October 2000.

[SvBvD$^+$01]   E Snoeks, A van Blaaderen, T van Dillen, C. M van Kats, K Velikov, M. L Brongersma, and A Polman. Colloidal assemblies modified by ion irradiation. *Nuclear Instruments and Methods in Physics Research Section B: Beam Interactions with Materials and Atoms*, 178(1–4):62–68, May 2001.

[TR95]   H. Trinkaus and A. I. Ryazanov. Viscoelastic Model for
             the Plastic Flow of Amorphous Solids under Energetic Ion
             Bombardment. *Physical Review Letters*, 74(25):5072–5075,
             June 1995.

[vDSF⁺01]   T van Dillen, E Snoeks, W Fukarek, C. M van Kats, K. P
             Velikov, A van Blaaderen, and A Polman. Anisotropic
             deformation of colloidal particles under MeV ion irradia-
             tion. *Nuclear Instruments and Methods in Physics Research
             Section B: Beam Interactions with Materials and Atoms*,
             175–177:350–356, April 2001.

[WKW04]   W. Wesch, A. Kamarou, and E. Wendler. Effect of high
             electronic energy deposition in semiconductors. *Nuclear In-
             struments & Methods in Physics Research Section B-Beam
             Interactions with Materials and Atoms*, 225(1-2):111–128,
             August 2004. WOS:000223792600010.